ISSN: 2414-1895 DOI: 10.6919/ICJE.202605_12(5).0023

Study on Hydraulic Performance of Modular Constructed Wetlands based on Baffle Optimization

Rong Hao, Zhonggou Chen*, Guoyi Zhang*

Department of Landscape and Architecture, Zhejiang Agriculture and Forestry University, Hangzhou 311300, China

Abstract

This study addresses the severe clogging, challenging construction quality control, and high maintenance costs associated with traditional constructed wetlands by exploring structural optimization approaches for modular constructed wetlands (MCW). To gain an intuitive understanding of the internal flow patterns within modular constructed wetlands, a three-dimensional CFD simplified porous medium model was developed using FLUENT software. To further optimize the hydraulic efficiency of the modular wetland system, the impact of baffle arrangement on overall hydraulic performance was systematically investigated. Nine baffle configuration modes were compared in simulations, revealing that a configuration with two inner baffles represented the optimal solution: it achieved a flow field uniformity index of 0.68, an effective volume ratio of 0.815, a hydraulic efficiency of 0.792, and a fluid dispersion coefficient of merely 0.028. Increasing the number of baffles or concentrating them inward significantly degraded the flow field, resulting in a hydraulic efficiency of only 0.441 for a configuration with four inner baffles. This study validates the effectiveness of CFD-based structural parameter optimization, providing a quantitative theoretical foundation and practical technical solutions for efficient, standardized design of modular constructed wetlands.

Keywords

Modular Constructed Wetlands; Numerical Simulation; Flow Field Distribution; Hydraulic Characteristics; Structural Optimization Design.

1. Introduction

Water constitutes an indispensable natural resource underpinning economic development and social well-being while ensuring global political stability. Nevertheless, accelerated population growth alongside rapid industrialization and agricultural expansion has precipitated unprecedented water scarcity and environmental degradation on a global scale. According to United Nations reports, over two billion people reside in water stressed nations and approximately 2.2 billion individuals lacked safely managed drinking water services in 2022[1]. This census includes 703 million people who remain without basic drinking water accessibility. Furthermore, a diverse array of contaminants comprising pathogens and nutrients along with heavy metals and emerging organic pollutants jeopardize aquatic ecosystems and public health across both developed and developing regions[2]. China has made substantial progress in water infrastructure but continues to encounter rigorous challenges stemming from pollution and ecosystem degradation as well as regional water scarcity. These multifaceted pressures necessitate the development of cost effective and resilient treatment technologies capable of deployment across diverse spatial scales.

In China, the Sponge City initiative launched in 2013 represents a comprehensive national effort to integrate green and gray infrastructure. This initiative aims to maintain post development runoff

ISSN: 2414-1895 DOI: 10.6919/ICJE.202605_12(5).0023

volume and peak flow below pre development levels while strengthening urban ecological resilience through infiltration and retention as well as purification and drainage[3]. As a vital component of this green gray infrastructure, constructed wetlands serve a critical function in regulating urban hydrology and purifying non point source pollution. By emulating the physical and chemical as well as biological synergies found in natural wetlands, constructed wetlands establish controlled ecosystems where substrates and plants and microorganisms interact to facilitate the migration and transformation of pollutants. These systems have demonstrated profound potential in treating domestic sewage and stormwater runoff along with mildly polluted water bodies across varied climatic and socioeconomic contexts.

Despite the widespread global application of constructed wetlands, traditional design approaches have demonstrated significant limitations in long-term engineering practice, severely restricting their operational lifespan and scalability[4]. The primary challenge hindering their stable operation is clogging. The continuous accumulation of suspended solids, organic matter, and microbial metabolites in substrate pores leads to reduced permeability coefficients, shortened hydraulic retention times, and the formation of "dead water zones," ultimately resulting in declining treatment efficiency or complete system failure[5]. Conventional clogging removal methods (e.g., localized excavation and material replacement) involve substantial engineering work, require system shutdown for maintenance, and only address symptoms rather than root causes. Additionally, traditional constructed wetlands predominantly employ cast-in-place civil engineering structures, which exhibit multiple drawbacks under this non-standardized "site-specific" construction model[6]. Firstly, construction timelines are highly susceptible to weather and geological conditions, making rapid delivery challenging. Secondly, quality control of cast-in-place structures (e.g., waterproof layer consistency, water distribution pipeline gradients) relies entirely on on-site construction capabilities, often leading to leakage or uneven water distribution[7]. Most critically, when deep clogging occurs, traditional clogging removal methods typically require large-scale mechanical excavation and material replacement, involving massive engineering work and system shutdown, which significantly increases maintenance costs throughout the entire life cycle[8,9].

To overcome the limitations of traditional constructed wetlands, modular constructed wetlands (MCW) have been proposed as an innovative technical approach. The core logic lies in deconstructing complex ecological treatment processes into standardized hardware units, achieving efficient engineering implementation through factory prefabrication and modular assembly. This design philosophy promises several key breakthroughs: Easy maintenance and renewal: Clogging modules can be quickly disassembled, replaced, or rotated to ensure continuous system operation; High construction efficiency: Factory prefabrication shortens construction periods and ensures quality control; Strong flexibility: Modules can be flexibly combined according to treatment requirements and site conditions; Resource recycling: The saturated substrate rich in organic matter can be reused as fertilizer or regenerated for reuse.

In light of this, this study focuses on modular constructed wetlands, aiming to achieve the following objectives: develop a three-dimensional CFD porous medium model for modular constructed wetlands; systematically simulate and evaluate the impact of different baffle distribution patterns on the hydraulic efficiency of module units; identify the optimal combination of structural parameters and propose an optimized design scheme for modular constructed wetlands; and provide a theoretical foundation and technical reference for advancing the scientific design, efficient application, and standardized development of modular constructed wetland technology.

2. Materials and Methods

2.1 Computational Fluid Dynamics (CFD) Simulation Technology

2.1.1 Fundamental Principles of CFD

As a critical branch of modern fluid mechanics, Computational Fluid Dynamics (CFD) integrates mathematics, computer science, and fluid mechanics to quantitatively describe the distribution of

ISSN: 2414-1895 DOI: 10.6919/ICJE.202605_12(5).0023

continuous physical quantities across time and space domains using discretized numerical methods[10]. The core of CFD technology lies in solving the system of partial differential equations governing fluid flow to obtain the spatio-temporal distribution of physical quantities such as velocity, pressure, and concentration, providing a theoretical and technical basis for understanding complex flow phenomena[11]. The basic CFD workflow is divided into three stages: pre-processing, solver calculation, and post-processing, each performing distinct functions[12].

Pre-processing is the foundational stage of CFD simulation, primarily including the construction of the geometric model, the partition of the computational grid, and the setting of boundary and initial conditions. Geometric models must be reasonably simplified based on the structural characteristics of the research object to reduce computational complexity while ensuring accuracy[13]. Mesh generation is a key step, as its quality directly determines subsequent calculation accuracy and efficiency. Grid density and distribution significantly impact the accuracy of results; local refinement is typically required in critical areas to capture fine-scale flow structures. By discretizing the research area, continuous physical space is divided into several discrete units, laying the foundation for numerical solutions.

Solver calculation is the core of CFD simulation, tasked with the numerical discretization and iterative solution of the control equations. This includes selecting control equations, determining discretization methods, choosing solution algorithms, and setting solver parameters and convergence criteria[14]. During the simulation, reasonable boundary and initial conditions (such as velocity inlets, pressure outlets, and wall boundaries) must be set based on actual working conditions to ensure physical validity. In the iterative process, a convergence residual standard is set[15]; the calculation is considered converged only when the residuals of monitored physical quantities fall below the preset threshold and global parameters like outlet flow rate stabilize.

Post-processing involves the visualization and data analysis of results to extract physically meaningful information from large numerical datasets. Post-processing software can generate various visualizations, such as velocity contours, streamlines, isotherms, and vector plots, to intuitively present the spatial distribution of physical quantities[16]. This analysis allows for the identification of key flow features-such as high-velocity regions, low-velocity stagnation zones, and vortex structures-revealing the internal mechanisms of flow phenomena. Post-processing results are critical for verifying simulation rationality and bridging numerical results with engineering insights.

Currently, common commercial CFD software in international academia and engineering includes FLUENT, PHOENICS, and CFX. ANSYS FLUENT has become a mainstream platform in hydraulic and environmental fluid mechanics due to its high accuracy, rich physical models, and good convergence. It offers various turbulence models, such as the $k-\epsilon$ and $k-\omega$ models, which are highly applicable for complex problems involving turbulence, heat transfer, and multiphase flows. This study utilizes ANSYS FLUENT 2022 R1 to ensure the accuracy and reliability of research results.

2.1.2 Governing Equations

The simulation assumes the fluid is incompressible, isothermal clean water, neglecting heat exchange. The flow follows the laws of mass conservation (continuity equation) and momentum conservation (Navier-Stokes equations).

Mass Conservation Equation (Continuity Equation):

$$\frac{\partial \rho}{\partial t} + \frac{\partial}{\partial x_i}(\rho u_i) = S_m \quad (1)$$

Where: ρ: Fluid density (kg/m^3), t: Time (s), u_i: Velocity vector component in the i direction (m/s), x_i: Spatial coordinate in the i direction (m), S_m: Mass source term ($kg/(m^3 \cdot s)$), representing fluid mass produced (positive) or lost (negative) per unit volume and tim.

ISSN: 2414-1895 DOI: 10.6919/ICJE.202605_12(5).0023

Momentum Conservation Equation (Navier-Stokes Equations):

$$\frac{\partial}{\partial t}(\rho u_i) + \frac{\partial}{\partial x_j}(\rho u_i u_j) = -\frac{\partial P}{\partial x_i} + \frac{\partial \tau_{ij}}{\partial x_j} + \rho g_i + S_i \quad (2)$$

Where: ρu_i: Momentum density in the i direction $(kg/(m^2 \cdot s))$, P: Static pressure (Pa), τ_{ij}: Stress tensor (Pa), ρg_i: Gravitational body force in the i direction (N/m^3), S_i: Additional momentum loss source term (N/m^3), typically consisting of viscous and internal resistance losses.

2.2 Hydraulic Simulation Methods for Constructed Wetlands

2.2.1 Porous Media Model

Substrate media in constructed wetlands are treated as porous media, where fluid movement is considered seepage flow. In CFD simulations, a porous media model describes the hydraulic characteristics of the substrate by adding a resistance source term (S_i) to the momentum equation. Porous media consist of a solid skeleton and volume spaces distributed with pores, which can be filled with liquid, gas, or multiphase fluids.

For isotropic uniform porous media, the resistance source term can be simplified as:

$$S_i = -\sum_{j=1}^{3} D_{ij}\mu u_j + \sum_{j=1}^{3} C_{ij}\frac{1}{2}\rho|u_j|u_j \quad (3)$$

Where D_{ij} and C_{ij} are the viscous and inertial resistance coefficient matrices, respectively. For simple uniform packing, it simplifies to:

$$S_i = -\left(\frac{\mu}{\alpha}u_i + C_2\frac{1}{2}\rho|u|u_i\right) \quad (4)$$

Where α is permeability and C_2 is the inertial resistance coefficient.

The Nash-Sutcliffe Efficiency (NSE) is a normalized statistic obtained by comparing the residual variance of simulation data with the variance of measured data, characterizing the 1:1 fit. The formula is:

$$NSE = 1 - \frac{\sum_{i=1}^{n}(Q_{oi}-Q_{si})^2}{\sum_{i=1}^{n}(Q_{oi}-\bar{Q}_o)^2} \quad (5)$$

Where Q_{oi} is the measured value, Q_{si} is the simulated value, and $\bar{Q}_o$ is the mean of all measured value. An NSE of 1 indicates a perfect simulation; results between 0 and 1 are acceptable, while values ≤ 0 indicate poor performance.

2.3 Hydraulic Performance Evaluation Indicators for Constructed Wetlands

To quantitatively analyze the hydraulic characteristics of modular constructed wetlands, this study employs indicators such as the effective volume ratio, standard flow dispersion, and hydraulic efficiency.

Theoretical Hydraulic Retention Time (T_n): Calculated under the ideal plug flow assumption, where fluid particles move at a uniform speed. It is the ratio of effective volume (V) to volumetric flow rate (Q):

$$T_n = V/Q \quad (6)$$

ISSN: 2414-1895 DOI: 10.6919/ICJE.202605_12(5).0023

Mean Residence Time (T_m): The average residence time of all fluid particles in the system. Unlike the ideal state, actual flow paths vary due to structure and media heterogeneity; T_m better reflects real hydraulic behavior.

Peak Residence Time (T_p): The time when tracer concentration reaches its maximum, often regarded as the actual hydraulic retention time. Discrepancies between these times (usually $T_p < T_m < T_n$) reflect short-circuiting or dead zones.

Effective Volume Ratio (e): Measures the relationship between the volume actively participating in flow and the theoretical design volume. When $e \approx 1$, space utilization is optimal; $e < 1$ indicates preferential flow, while $e > 1$ suggests significant dead zones.

$$e=\frac{V_e}{V_t \cdot n} \tag{7}$$

V_e: Effective volume (m^3); V_t: Total volume; n: Porosity.

Standard Fluid Dispersion (σ_θ^2): Quantifies the degree of fluid dispersion. Values range from 0 to 1; smaller values indicate more uniform distribution and better hydraulic performance[41].

$$\sigma_t^2 = \frac{\int_0^\infty (t-t_m)^2 \cdot N(t)dt}{\int_0^\infty N(t)dt} \tag{8}$$

$$\sigma_\theta^2 = \frac{\sigma_t^2}{T_n^2} \tag{9}$$

Hydraulic Efficiency (λ): A comprehensive indicator reflecting fluid uniformity, ranging from 0 to 1.

$$\lambda = e(1-\sigma_\theta^2) \tag{10}$$

Pollutant Removal Efficiency (η): Directly reflects the treatment effect for pollutants like COD, TP, and TN.

$$\eta = \frac{S_0-S_t}{S_0} \times 100\% \tag{11}$$

2.4 Numerical Model Construction for Modular Constructed Wetlands

The geometric models employed in this study were constructed using ANSYS Workbench 2022 R1 software. During model processing, the porous medium region (i.e., the filler zone) was simplified into a uniform solid, with its hydraulic characteristics defined by subsequent parameter settings for the porous medium model[17]. In the pre-simulation preparation phase, the three-dimensional geometric model of the system was established using ANSYS SpaceClaim. The modular constructed wetland system was modeled with dimensions of 3000 mm in length, 1000 mm in width, and 900 mm in height, maintaining a geometric scale consistent with the physical experimental setup to ensure comparability between numerical simulation results and experimental data.

Grid partitioning is a critical step in numerical simulation, as its quality directly impacts the accuracy and computational efficiency of the results. This study employed the ANSYS Meshing software for grid partitioning, utilizing tetrahedral elements to discretize the computational domain with localized grid refinement in pore and wall-surface regions to capture fine-scale flow field structures. To evaluate the influence of grid density on computational outcomes, grid independence analysis was conducted. By comparing results across different grid sizes, the optimal grid size of 0.008 m was

ISSN: 2414-1895 DOI: 10.6919/ICJE.202605_12(5).0023

determined, yielding a total model grid count of approximately 750,000. At this grid density, the computational results stabilized, with grid accuracy meeting simulation requirements[18].

Regarding the simulation setup and post-processing procedures, the inlet is positioned at the upper part of one side wall of the module, with the boundary condition type selected as "velocity inlet." Calculated based on the designed hydraulic load of 0.5 m/d, the inlet velocity is approximately 5.79×10^{-6}m/s. Considering potential flow fluctuations during actual operation and to more clearly illustrate flow field variations, the inlet velocity was appropriately increased to 0.001 m/s in the simulation while maintaining the Reynolds number within an appropriate range. Relevant studies indicate that flow characteristics at this velocity level align with those under low-velocity conditions, yielding more stable numerical solutions[19]. The outlet is located at the bottom of the opposite side wall of the module, with the boundary condition type set as "pressure outlet" and a gauge pressure of 0 Pa. For porous wall regions, all other module walls and bottom surfaces-excluding the designated inlet and outlet areas-are defined as "internal interfaces," where the pore effects have been incorporated through geometric modeling, allowing free fluid passage.

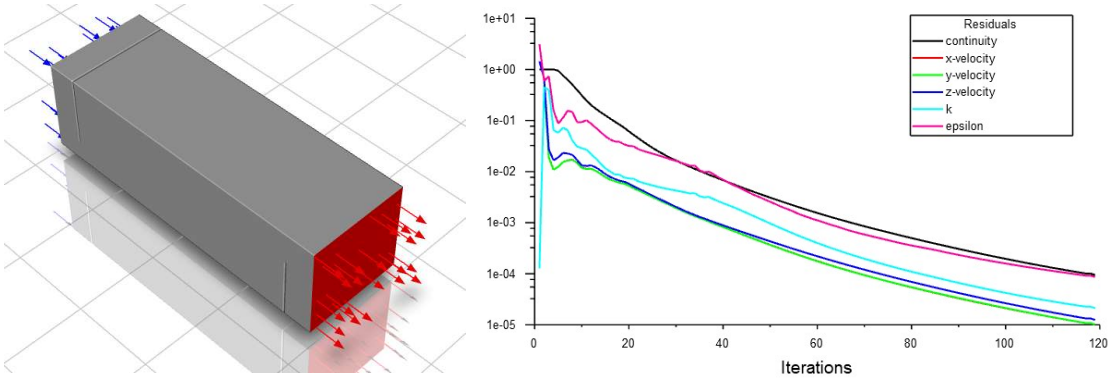

Figure 1. Numerical Model and Residual Monitoring Chart

3. Analysis of Hydraulic Characteristics of Modular Constructed Wetlands under Different Baffle Layouts

3.1 Qualitative Analysis of Flow Fields and Streamlines

To visually analyze the impact of different baffle installation configurations on the flow field patterns within modular constructed wetlands, this study extracted velocity cloud diagrams (Figure 2) and flowline diagrams (Figure 3) obtained after stable operation under nine operational conditions. In the velocity cloud diagrams, colors transition from red to blue, indicating decreasing flow velocities, while the flowline diagrams illustrate the movement trajectories of water particles.

From the perspective of flow field distribution characteristics, Condition 1 exhibits a high-speed zone primarily concentrated near the inlet and baffle gaps, with low-speed zones distributed in system corners. The overall flow lines remain relatively smooth, though localized flow deviations are observed. Condition 2 shows a narrower high-speed zone compared to Condition 1, with flow lines exhibiting slight curvature near the baffles, indicating effective disturbance generated by the baffles. Condition 3 demonstrates the most extensive high-speed zone with more uniform flow lines and significantly reduced low-speed areas, exhibiting markedly superior flow field uniformity than the previous two conditions. When the number of baffles increases to three, Conditions 4, 5, and 6 all display varying degrees of high-speed channels and low-speed retention zones. Specifically, the three inner baffles in Condition 6 form distinct local vortices within the system, accompanied by flow line entanglement and fragmentation, expanding the dead zone. The flow field uniformity in Conditions 4 and 5 also declines compared to the two-baffle configuration. With four baffles, Conditions 7 and 8 exhibit further expansion of high-speed regions but more chaotic flow lines with localized backflows. Condition 9 shows severe deterioration, featuring extensive blue-colored low-speed zones

ISSN: 2414-1895 DOI: 10.6919/ICJE.202605_12(5).0023

on velocity maps and extremely sparse, discontinuous flow lines, indicating the formation of significant stagnant water areas where water flow becomes nearly impossible.

Upon completion of the computational analysis, the report extracted data to calculate the average flow velocity, standard deviation, and flow field uniformity index (UDI) for each operating condition, with the results summarized in Table 1.

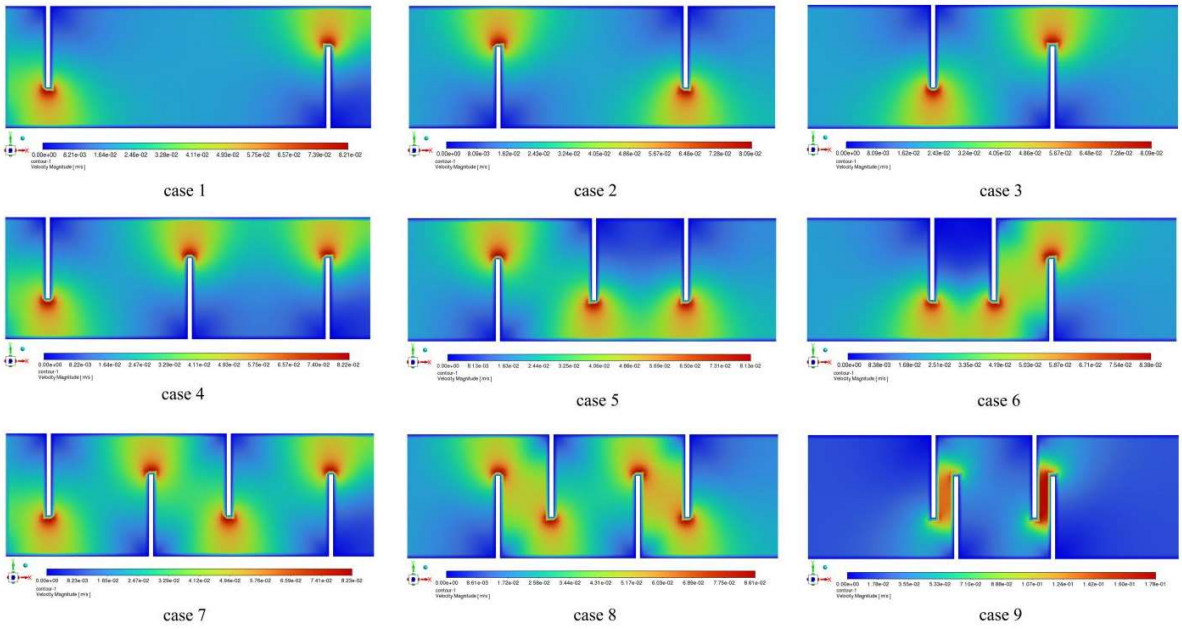

Figure 2. Flow Field Diagrams of Nine Baffle Operating Conditions

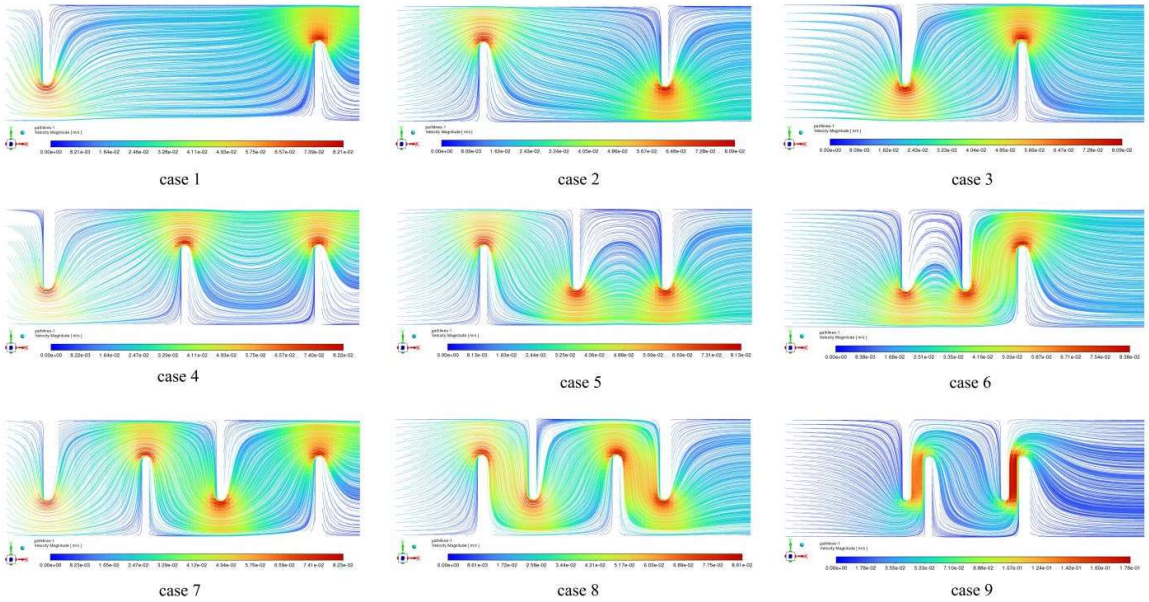

Figure 3. Streamline Diagrams of Nine Baffle Operating Conditions

Analysis of the average flow velocity shows that the values range from 2.39×10^{-2} m/s to 3.15×10^{-2} m/s across all operating conditions. Condition 2 exhibits the lowest average velocity at 2.39×10^{-2} m/s, while Condition 9 records the highest at 3.15×10^{-2} m/s. Overall, an evident upward trend in average velocity is observed with increased baffle counts: conditions with four baffles generally demonstrate higher velocities than those with two or three baffles, as the additional baffles reduce the cross-sectional flow area and consequently increase local velocity.

ISSN: 2414-1895 DOI: 10.6919/ICJE.202605_12(5).0023

From the standard deviation analysis, the standard deviation reflects the degree of dispersion in the flow velocity distribution; a higher value indicates a more uneven distribution. Under Condition 3, the standard deviation was the smallest at 0.87×10^{-2} m/s, indicating the most stable flow field; under Condition 9, the standard deviation was the largest at 2.91×10^{-2} m/s, reflecting extremely high velocity dispersion. The standard deviations under the two-plate condition were generally lower than those under the three-and four-plate conditions, suggesting that increasing the number of plates exacerbates velocity distribution unevenness. Notably, the standard deviation under Condition 9 far exceeded that of all other conditions, indicating that the arrangement of the four inner plates severely compromised flow field uniformity.

Table 1. Uniformity Indicators of Flow Fields under Nine Operating Conditions

Case No.	Baffle Position	Baffle Count	Avg. Velocity (10^{-2}m/s)	Std. Deviation (10^{-2}m/s)	UDI
Case 1	Outer	2	2.56	1.01	0.61
Case 2	Middle	2	2.39	0.97	0.59
Case 3	Inner	2	2.76	0.87	0.68
Case 4	Outer	3	2.54	1.26	0.50
Case 5	Middle	3	2.55	1.25	0.51
Case 6	Inner	3	2.57	1.31	0.49
Case 7	Outer	4	2.95	1.27	0.57
Case 8	Middle	4	3.12	1.35	0.56
Case 9	Inner	4	3.15	2.91	0.07

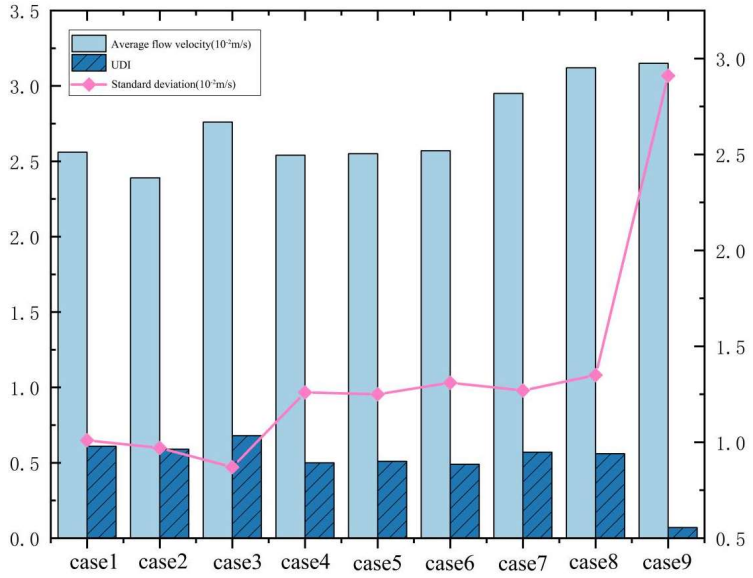

Figure 4. Bar Chart of Flow Field Uniformity Indicators under Nine Operating Conditions

ISSN: 2414-1895 DOI: 10.6919/ICJE.202605_12(5).0023

The UDI (Uniformity Index) is a commonly used metric for evaluating flow field uniformity, physically representing the degree of uniformity in velocity distribution—higher values closer to 1 indicate more uniform velocity distribution. Among the nine test conditions, Condition 3 achieved the highest UDI of 0.68, followed by Conditions 1 and 7 with values of 0.61 and 0.57, respectively. Condition 9 recorded the lowest UDI of 0.07, indicating extremely uneven flow field under this condition. The UDI values for the two-plate configuration were generally higher than those for the three-and four-plate configurations, suggesting that within the studied plate arrangement range, two plates better maintain flow field uniformity. Regarding plate positioning, the inner side configuration yielded the best results with a UDI of 0.68, whereas the three-and four-plate configurations performed worst (UDI values of 0.49 and 0.07 respectively), indicating an optimal threshold for inner plate quantity beyond which flow field quality deteriorates significantly.

In summary, based on the flow field distribution characteristics, the flow field under condition 3 with two inner baffles exhibits the most uniform distribution, featuring continuous flow in the high-speed zone, minimal turbulence in the low-speed zone, and smooth flow lines. When the number of baffles increases to three, the flow field becomes turbulent; with four inner baffles, extensive water stagnation zones occur. In terms of uniformity metrics, condition 3 demonstrates the highest UDI, effective volume ratio, and hydraulic efficiency, along with the lowest fluid dispersion, significantly outperforming other conditions. Therefore, two inner baffles represent the optimal configuration; the number of baffles should not exceed two, and their placement should avoid concentration on the inner side.

3.2 Quantitative Analysis of Hydraulic Characteristics

To conduct an in-depth comparative analysis of the hydrodynamic characteristics of nine baffle wetland models, this study calculated particle residence times through numerical simulation experiments to evaluate their hydraulic performance under various operating conditions. The simulation results were exported as.dpm files, and the average hydraulic residence time was calculated using Excel. The Nash-Sutcliffe efficiency coefficient (NSE) was employed to assess model accuracy, while the fitting quality was quantified by comparing the residual variance with the measured variance. Detailed results are presented in Table 2.

Table 2.Hydrodynamic Characteristics Data Table for Nine Operating Conditions

Case No.	T_n(s)	T_m(s)	e	λ	σ_θ^2
Case 1	18612	14856	0.798	0.767	0.038
Case 2	18612	14375	0.771	0.743	0.035
Case 3	18612	15175	0.815	0.792	0.028
Case 4	18612	13112	0.704	0.662	0.059
Case 5	18612	13279	0.713	0.671	0.058
Case 6	18612	13576	0.729	0.682	0.064
Case 7	18612	12878	0.691	0.649	0.060
Case 8	18612	13983	0.751	0.699	0.068
Case 9	18612	12014	0.645	0.441	0.316

ISSN: 2414-1895 DOI: 10.6919/ICJE.202605_12(5).0023

Analysis of the effective volume ratio (e) reveals its reflection of spatial utilization efficiency within wetland systems: a higher e value closer to 1 indicates smaller dead zones and more uniform water flow distribution. In the two-panel configuration (conditions 1–3), e values ranged from 0.771 to 0.815, with condition 3 achieving the highest value of 0.815 and condition 2 the lowest of 0.771, yielding an average effective volume ratio of 0.795. The three-panel configuration (conditions 4–6) exhibited e values between 0.704 and 0.729, averaging 0.715-a reduction of approximately 10% compared to the two-panel setup. The four-panel configuration (conditions 7–9) showed e values ranging from 0.645 to 0.751, averaging 0.696, with condition 9 recording the lowest value of 0.645, representing a 20.9% decrease from condition 3. These results demonstrate that the two-panel configuration achieves optimal spatial utilization, while increased panel numbers reduce the effective volume ratio. Specifically, condition 3 exhibits the smallest dead zone and most efficient spatial utilization, whereas condition 9 demonstrates the largest dead zone and significant effective volume loss.

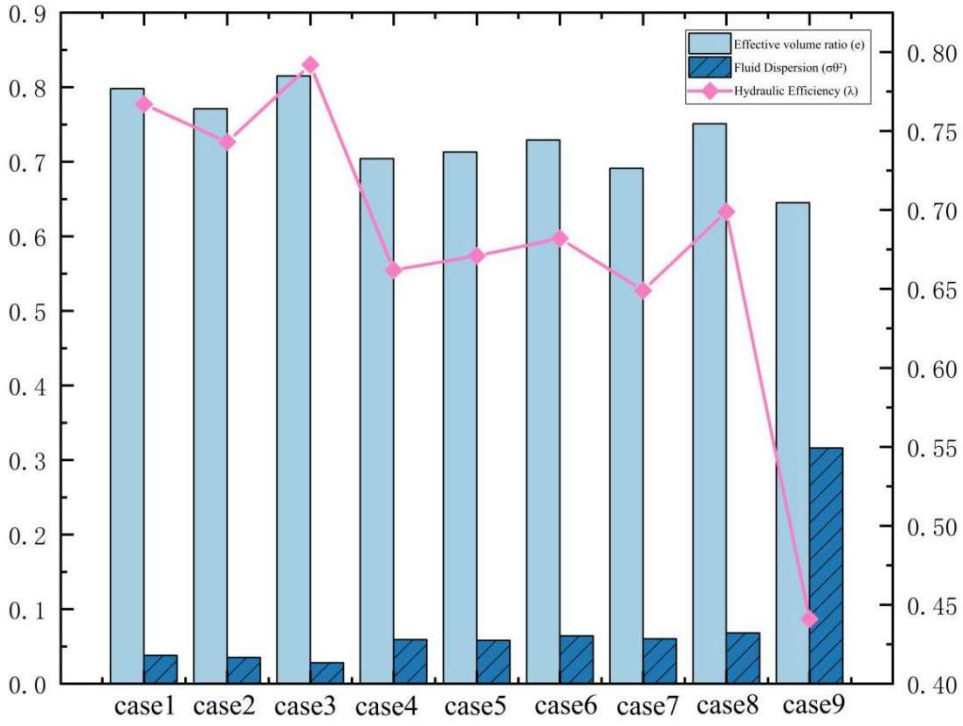

Figure 5. Bar Chart of Hydraulic Characteristic Indicators under Nine Operating Conditions

Analyzing fluid dispersion ($\sigma\theta^2$), this parameter reflects the degree of dispersion in residence time distribution: lower values indicate closer alignment with ideal plug flow conditions, with reduced short-circuiting and dead zone phenomena. In the two-baffle configuration, $\sigma\theta^2$ ranged from 0.028 to 0.038-0.028 in Configuration 3, 0.038 in Configuration 1, 0.035 in Configuration 2, and an average of 0.034. The three-baffle configuration exhibited $\sigma\theta^2$ between 0.058 and 0.064, averaging 0.060-a 76% increase compared to the two-baffle setup. In the four-baffle configuration, $\sigma\theta^2$ was 0.060 in Configuration 7 and 0.068 in Configuration 8, while Configuration 9 reached 0.316. Excluding Configuration 9 yields an average of 0.064, representing an 88% improvement over the two-baffle setup; its dispersion was 11.3 times higher than in Configuration 3. Thus, the two-baffle configuration demonstrates the lowest flow dispersion and most plug-like flow behavior, whereas Configuration 9's abnormally high dispersion indicates severe short-circuiting and dead zones caused by the inner four baffles, resulting in highly uneven residence time distribution.

From the perspective of hydraulic efficiency (λ), this metric integrates the effective volume ratio and fluid dispersion degree, serving as the core indicator for evaluating overall wetland hydraulic

ISSN: 2414-1895 DOI: 10.6919/ICJE.202605_12(5).0023

performance. A higher λ value indicates superior hydraulic performance. Under the two-panel baffle configuration, λ ranged from 0.743 to 0.792, with condition 3 achieving the highest value of 0.792, followed by condition 1 at 0.767, and condition 2 at the lowest 0.743, averaging 0.767. In the three-panel configuration, λ ranged between 0.662 and 0.682, averaging 0.672-a 12.4% decrease compared to the two-panel configuration. For the four-panel configuration, conditions 7 and 8 exhibited λ values of 0.649 and 0.699 respectively, while condition 9 recorded only 0.441. Excluding condition 9 yields an average of 0.674, representing a 12.1% decline from the two-panel configuration; condition 9 also showed a 44.3% decrease compared to condition 3. Condition 3 demonstrated the highest hydraulic efficiency at 0.792, significantly outperforming other configurations, whereas condition 9's lowest efficiency of 0.441 indicates that the arrangement of the four inner baffles severely compromised hydraulic performance.

Analysis of the hydraulic performance under nine operating conditions reveals that configurations with two baffles exhibit superior overall hydraulic performance compared to those with three or four baffles. Specifically, the configuration with two baffles on the inner side demonstrates the highest effective volume ratio and hydraulic efficiency, along with the lowest fluid dispersion and most uniform flow field. Increasing the number of baffles or concentrating them on the inner side significantly degrades hydraulic performance; notably, the configuration with four baffles on the inner side (configuration 9) shows the poorest performance across all metrics.

4. Conclusion

Through a comprehensive analysis of flow velocity contour maps, flowline diagrams, uniformity indices, and hydraulic performance metrics under nine baffle installation scenarios, the optimal baffle configuration scheme for modular constructed wetland systems can be determined.

Based on the flow field distribution characteristics, the overall flow performance under the two-baffle configuration is superior to that of the three-and four-baffle configurations. Specifically, the high-speed region under the two-baffle configuration exhibits uniform and continuous distribution, while the low-speed region is compressed to a minimal corner area with smooth, non-winding flow lines and no significant short-circuiting or stagnant water zones. In contrast, the three-baffle configuration shows localized vortices and flow line curvature, whereas the four-baffle configuration demonstrates significantly deteriorated flow fields-particularly configuration 9 with four inner baffles, which creates extensive stagnant water zones, sparse and fragmented flow lines, and substantially reduced effective flow capacity.

Regarding hydraulic performance metrics, the effective volume ratio (e) of the two-baffle configuration ranges from 0.771 to 0.815, the hydraulic efficiency (λ) from 0.743 to 0.792, and the fluid dispersion degree ($\sigma\theta^2$) from 0.028 to 0.038-all significantly outperforming the three-baffle and four-baffle configurations. Specifically, the two-baffle inner configuration (3) achieves the highest effective volume ratio (0.815), maximum hydraulic efficiency (0.792), and minimum fluid dispersion degree (0.028), indicating optimal spatial utilization, the most concentrated residence time distribution, and superior overall hydraulic performance. In contrast, the four-baffle inner configuration (9) demonstrates only an effective volume ratio of 0.645, hydraulic efficiency of 0.441, and fluid dispersion degree of 0.316, with all metrics markedly inferior to the other configurations.

In conclusion, the configuration with two inner baffles under operating condition 3 represents the optimal baffling arrangement among the nine scenarios. This design effectively guides water flow, suppresses short-circuiting, reduces dead zones, enhances spatial utilization efficiency, and significantly improves the hydraulic performance of the modular constructed wetland system. For this structural model, it is recommended to use no more than two baffles, preferably arranged on the inner side; concentrated placement of multiple baffles on the inner side should be avoided to prevent flow field deterioration.

Several limitations of this study should be acknowledged. First, the CFD simulations assumed clean water and idealized boundary conditions while neglecting biofilm growth and suspended solids

ISSN: 2414-1895 DOI: 10.6919/ICJE.202605_12(5).0023

accumulation. These factors may alter the permeability gradient over time through clogging. Second, the experimental validation was conducted under controlled laboratory conditions using a simplified module configuration. Consequently, long term performance under real world influent conditions, such as variable flow and high suspended solids as well as seasonal temperature fluctuations, remains to be evaluated. Third, the porous medium was modeled as isotropic with constant resistance coefficients, whereas actual substrates may exhibit spatial heterogeneity due to uneven packing or biological growth.

Future research should extend these findings in several strategic directions. One priority is the pilot scale testing of combined modules under dynamic hydraulic loading and actual wastewater to validate long term operational stability. Another direction involves the incorporation of biofilm growth and clogging evolution into the CFD model to predict changes in permeability and inform maintenance schedules. Additionally, researchers should couple hydraulic optimization with biochemical reaction models, such as Monod kinetics for nitrogen removal, to assess the balance between flow uniformity and the redox stratification necessary for denitrification. Finally, the development of simplified design nomograms or empirical equations based on these CFD results could enable the rapid configuration of modular wetlands for different treatment targets without the need for extensive simulation.

References

[1] United Nations Children's Fund, World Health Organization. Progress on household drinking water, sanitation and hygiene 2000-2022: special focus on gender[M]. World Health Organization, 2024.

[2] Schwarzenbach R P, Egli T, Hofstetter T B, et al. Global water pollution and human health[J]. Annual review of environment and resources, 2010, 35: 109-136.

[3] Fletcher T D, Shuster W, Hunt W F, et al. SUDS, LID, BMPs, WSUD and more–The evolution and application of terminology surrounding urban drainage[J]. Urban water journal, 2015, 12(7): 525-542.

[4] Suhaib K H, Bhunia P. Dynamics of clogging in subsurface flow constructed wetlands[J]. Journal of Hazardous, Toxic, and Radioactive Waste, 2022, 26(1): 03121004.

[5] Vymazal J. Constructed wetlands for wastewater treatment: five decades of experience[J]. Environmental science & technology, 2011, 45(1): 61-69.

[6] Fang Y, Kong L, Zhang P, et al. Fifteen-year analysis of constructed wetland clogging: A critical review[J]. Journal of Cleaner Production, 2022, 365: 132755.

[7] Zhong H, Jiang C, He X, et al. Simultaneous change of microworld and biofilm formation in constructed wetlands filled with biochar[J]. Journal of Environmental Management, 2024, 349: 119583.

[8] Li Y, Peng L, Li H, et al. Clogging in subsurface wastewater infiltration beds: genesis, influencing factors, identification methods and remediation strategies[J]. Water Science and Technology, 2021, 83(10): 2309-2326.

[9] Rajabzadeh A R, Legge R L, Weber K P. Multiphysics modelling of flow dynamics, biofilm development and wastewater treatment in a subsurface vertical flow constructed wetland mesocosm[J]. Ecological engineering, 2015, 74: 107-116.

[10] Zhang Hui. Simulation study on indoor pollutant diffusion concentration fields based on multi-factor coupling [D]. Chongqing Jiaotong University, 2011.

[11] Yin Decai. Simulation study of horizontal subsurface flow constructed wetlands based on CFD [D]. Hunan University, 2017.

[12] Anle, Li Qingman, Liang Jie, et al. Research and Application of CFD in Urban Wind and Heat Environment in China [J]. Journal of Aerodynamics, 2024,42(3):1-18.

[13] Li Lei, Hu Fei, Liu Jing. Application of CFD technology in mesoscale issues of urban climate and environment in China [J]. Progress in Meteorological Science and Technology, 2015,5(6):23-30.

[14] Zhang Xin, Yang Gang, Wang Zhiqiang, et al. Numerical simulation of turbulent flow in curved flue tubes based on CFD [J]. Industrial Furnace, 2023,45(1):6–11+15.

ISSN: 2414-1895 DOI: 10.6919/ICJE.202605_12(5).0023

[15] Alexandros T, Steve M, John B. Computational fluid dynamics modelling of different detention pond configurations in the interest of sustainable flow regimes and gravity sedimentation potential[J]. Water and Environment Journal, 2015, 29(1): 129-139.

[16] Wang Bingjie, Li Hui, Yang Xiaoyong, et al. Application progress of CFD numerical simulation technology in studying the multiphase flow characteristics of droplet microfluidics [J]. Chemical Industry Progress, 2021,40(4):1715.

[17] Klaywittaphat P ,Promping J ,Chatthong B .Optimizing variable Geometry of SMBI nozzle for Thailand Tokamak 1 (TT-1) using CFD with Ansys (Fluent)[J].Fusion Engineering and Design,2026,223115556-115556.

[18] Patil M ,Sidramappa A ,Hebbale M A , et al.Computational fluid dynamics (CFD) analysis of air-cooled solar photovoltaic (PV/T) panels[J].Materials Today: Proceedings,2024,10093-101.

[19] Banik A ,Bandyopadhyay K T ,Biswal K S .Computational Fluid Dynamics (CFD) Simulation of Cross-flow Mode Operation of Membrane for Downstream Processing[J].Recent Patents on Biotechnology,2019, 13(1):57-68.